EGIBILITY NOTICE

A major purpose of the Technical Information Center is to provide the broadest dissemination possible of information contained in DOE's Research and Development Reports to business, industry, the academic community, and federal, state and local governments.

Although a small portion of this report is not reproducible, it is being made available to expedite the availability of information on the research discussed herein.

LA-UR - 83-1388

ConF-830469--4

Los Alamos National Laboratory is operated by the University of California for the United States Department of Energy under contract W-7405-ENG-36

MASTER

LA-UR--83-1388

DE83 012670

TITLE: DYNAMICAL FUSION THRESHOLDS IN MACROSCOPIC AND MICROSCOPIC THEORIES

AUTHOR(S): Thomas R. Davies, Physics Division, Oak Ridge National Laboratory
Arnold J(ohn) Sierk, T-9
J(ames) Rayford Nix, T-9

SUBMITTED TO: Proceedings of Conference on Nuclear Physics with Heavy Ions
Stony Brook, New York, April 14-16, 1983

DISCLAIMER

Los Alamos Los Alamos National Laboratory
Los Alamos, New Mexico 87545

FORM NO 836 R4
ST NO 2629 5/81

DYNAMICAL FUSION THRESHOLDS IN MACROSCOPIC AND MICROSCOPIC THEORIES

K. Thomas R. Davies
Physics Division, Oak Ridge National Laboratory
Oak Ridge, Tennessee 37830

Arnold J. Sierk
Theoretical Division, Los Alamos National Laboratory
Los Alamos, New Mexico 87545

J. Rayford Nix
Theoretical Division, Los Alamos National Laboratory
Los Alamos, New Mexico 87545

to be published in

Proceedings of Conference on
Nuclear Physics with Heavy Ions

Stony Brook, New York

April 14-16, 1983

DYNAMICAL FUSION THRESHOLDS IN MACROSCOPIC AND MICROSCOPIC THEORIES*

K. THOMAS R. DAVIES
Physics Division, Oak Ridge National Laboratory
Oak Ridge, Tennessee 37830

ARNOLD J. SIERK
Theoretical Division, Los Alamos National Laboratory
Los Alamos, New Mexico 87545

J. RAYFORD NIX
Theoretical Division, Los Alamos National Laboratory
Los Alamos, New Mexico 87545

Macroscopic and microscopic results demonstrating the existence of dynamical fusion thresholds are presented. For macroscopic theories, it is shown that the extra-push dynamics is sensitive to some details of the models used, e.g. the shape parametrization and the type of viscosity. The dependence of the effect upon the charge and angular momentum of the system is also studied. Calculated macroscopic results for mass-symmetric systems are compared to experimental mass-asymmetric results by use of a tentative scaling procedure, which takes into account both the entrance-channel and the saddle-point regions of configuration space. Two types of dynamical fusion thresholds occur in TDHF studies: (1) the microscopic analogue of the macroscopic extra push threshold, and (2) the relatively high energy at which the TDHF angular momentum window opens. Both of these microscopic thresholds are found to be very sensitive to the choice of the effective two-body interaction.

*Research supported by the U.S. Department of Energy under a contract with the University of California and Contract W-7405-eng-26 with the Union Carbide Corporation.

K.T.R. DAVIES, A.J. SIERK and J.R. NIX

1. INTRODUCTION

Since a wide variety of theories and models have been developed in order to understand heavy-ion reactions, it is interesting to explore the relationships between different theoretical approaches. While formal connections between different methods are usually obscure, it is possible for two theories to give quite consistent agreement — qualitatively if not quantitatively — regarding a particular type of reaction. In this paper we shall demonstrate that two quite different theories qualitatively predict very similar behavior for heavy-ion fusion. Specifically, we shall discuss dynamical fusion thresholds, which are predicted in various macroscopic models[1-5] and also in microscopic TDHF theory.[6-10]

This paper is structured as follows. In Section 2 we introduce the concept of a dynamical fusion threshold. Section 3 presents recent macroscopic studies[5] which demonstrate the sensitivity of the extra-push threshold to various details of the model, particularly the viscosity mechanism. Then, in Section 4 we discuss the TDHF fusion thresholds, which include both the extra-push threshold and the angular momentum window, and we show the sensitivity of these thresholds to changes in the effective two-body interaction.[9,11] Finally, Section 5 gives a brief summary of our results.

2. DYNAMICAL FUSION THRESHOLDS

The concept of an additional energy for fusion, or an extra push,[1-5] is illustrated schematically in Fig. 1. In this figure, E_B is the maximum value of the interaction barrier for one-dimensional (radial) motion in the entrance channel,

DYNAMICAL FUSION THRESHOLDS

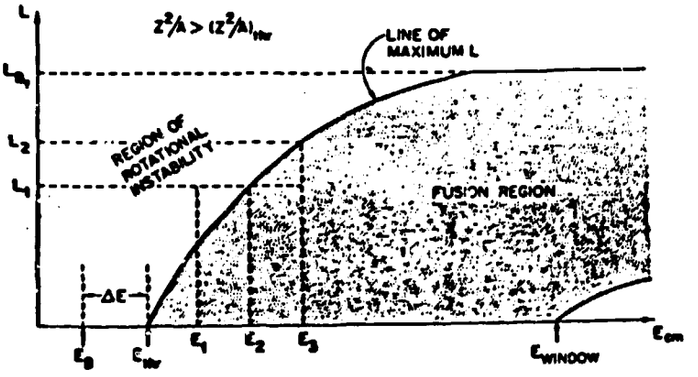

FIGURE 1 Typical fusion region in the CM energy, angular momentum plane. The figure contains features occurring in both macroscopic and microscopic studies. The angular momentum L_{B_f} is the angular momentum for which the fusion barrier vanishes.

and the threshold E_{thr} is the minimum energy for which one obtains fusion for head-on collisions. Now for light systems, if subbarrier fusion is neglected, these two energies are identical. Then if the charge on the system is increased, the threshold energy increases since more energy is required for fusion. However, E_B also increases with charge so that E_{thr} and E_B coincide until we reach some critical fissility designated by $(Z^2/A)_{thr}$, after which E_{thr} increases faster than E_B. In this picture $Z^2/A > (Z^2/A)_{thr}$ and $\Delta E = E_{thr} - E_B$ is the additional energy above the barrier required to give fusion for head-on collisions.

We note that Fig. 1 shows a relatively high-energy threshold E_{window} where fusion abruptly disappears for L = 0. This is the TDHF angular momentum window.[6,9] This threshold is also of dynamical origin, but it is completely different from the extra-push threshold shown at the lower energy. It is intimately associated with the transparency inherent in the mean-field approximation, and its existence

has not been verified experimentally.[11]

3. MACROSCOPIC CALCULATIONS

One of the main lessons that we have learned about fusion behavior is that, as the angular momentum or the charge on the system increases, it becomes more difficult to describe the dynamics by simple one-dimensional models.[1-5] Thus, macroscopic calculations should ideally be done using a general set of collective coordinates, and it is convenient to project from this multidimensional configuration space several simple coordinates which have special physical significance. For our studies,[5] these projected coordinates are denoted by r, which gives the distance between the mass centers of the ions, and σ, which is a measure of fragment elongation (or necking). The specific model that we use is an axially symmetric shape consisting of smoothly joined portions of three quadratic surfaces of revolution.[12] The coordinates r and σ are then defined in terms of moments of the nuclear shape.[5,13] For mass-symmetric reactions, r and σ are given by

$$r = 2\langle z \rangle, \tag{1}$$

$$\sigma = 2[\langle z^2 \rangle - \langle z \rangle^2]^{1/2}, \tag{2}$$

where z is measured along the symmetry axis and the angular bracket denotes an average over the half volume to the right of the midplane of the body.

The dynamical trajectories are obtained by solving the classical Hamilton's equations of motion, which have been generalized to include viscosity[13]:

$$\dot{q}_i = \frac{\partial \mathcal{H}}{\partial p_i}, \qquad i = 1,2,\ldots N, \tag{3}$$

$$\dot{p}_i = -\frac{\partial H}{\partial q_i} - \frac{\partial F}{\partial \dot{q}_i}, \qquad i = 1,2,\ldots N, \qquad (4)$$

where q_i and p_i are a collective coordinate and its conjugate momentum and

$$H = T + V. \qquad (5)$$

The potential energy V is the sum of the Coulomb electrostatic energy and a nuclear macroscopic energy

$$V(q) = V_{coul}(q) + V_{nucl}(q), \qquad (6)$$

while T is the collective kinetic energy and F is the Rayleigh dissipation function.

In Fig. 2 we display a potential-energy contour map for

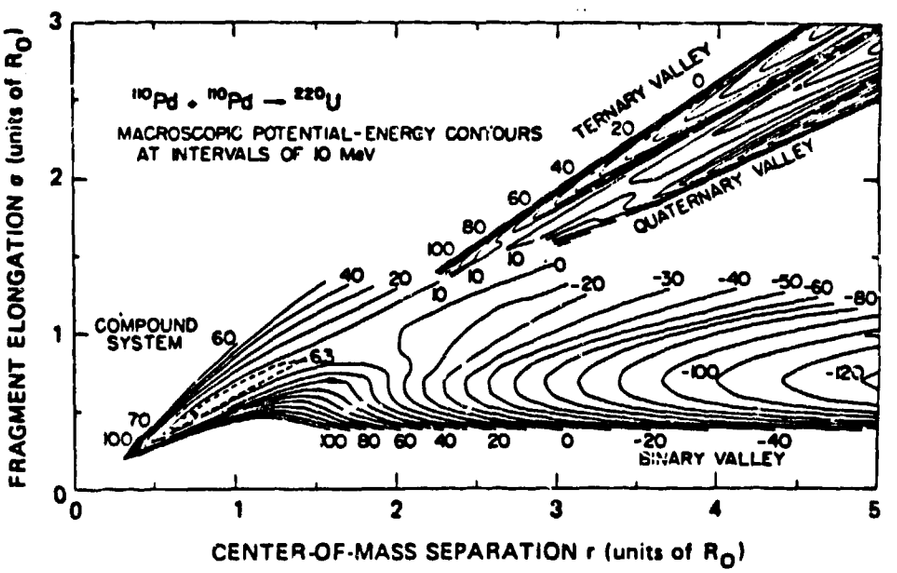

FIGURE 2 Potential-energy contours, in units of MeV, for the reaction $^{110}Pd + ^{110}Pd \rightarrow ^{220}U$, calculated with a single-Yukawa macroscopic model.[14] The location of the sphere is given by the solid point, and the location of two touching spheres is given by two adjacent solid points.

the head-on collision of $^{110}Pd + {}^{110}Pd \rightarrow {}^{220}U$. Initially, the two separated spherical ^{110}Pd nuclei move up the binary valley, near the bottom of the figure, and come into hard contact at the point indicated by the two adjacent circles. This point is slightly inside the maximum in the one-dimensional interaction barrier, but is on the side of a steep hill with respect to fragment elongation. The saddle point of the combined system is located at the intersection of the dashed 6.3-MeV contours. The criterion that we have adopted for compound-nucleus formation is that the dynamical trajectory passes to the left of the saddle, so that the system becomes trapped in the potential-energy hollow surrounding the sphere. If the trajectory passes to the right of the saddle point, the system reseparates in a deep-inelastic reaction.

Figure 3 illustrates typical dynamical trajectories in the r, σ plane for various values of ΔE, which is the difference between the CM energy and the maximum in the one-dimensional interaction barrier. This figure shows that as the bombarding energy increases, the trajectories are displaced to the left, giving rise to more compressed shapes. The trajectories for $\Delta E = 0.5$ and 20 MeV do not fuse, while $\Delta E = 90$ MeV is the threshold value, or minimum ΔE required for fusion, since its trajectory just passes through the saddle point of the combined system.

In Fig. 4 we compare dynamical trajectories for five different types of dissipation: zero dissipation, ordinary two-body viscosity with a viscosity coefficient of .02 TP,[13,17] one-body wall-formula dissipation,[18-19] one-body wall-and-window dissipation,[17-19] and pure window dissipation. The dynamical paths for no dissipation and two-body viscosity prefer changes in separation r rather

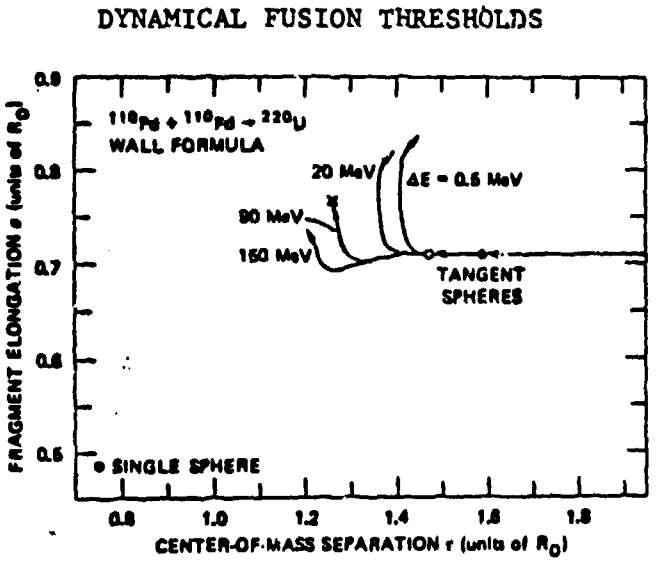

FIGURE 3 Effect of bombarding energy on dynamical trajectories in the r-σ plane for the head-on collision, $^{110}Pd + ^{110}Pd \rightarrow ^{220}U$, calculated for wall-formula dissipation. Here, and in Figs. 4-6, the saddle-point configuration for the combined system is indicated by a cross (×), and the nuclear macroscopic energy is the Yukawa-plus exponential model.[15,16]

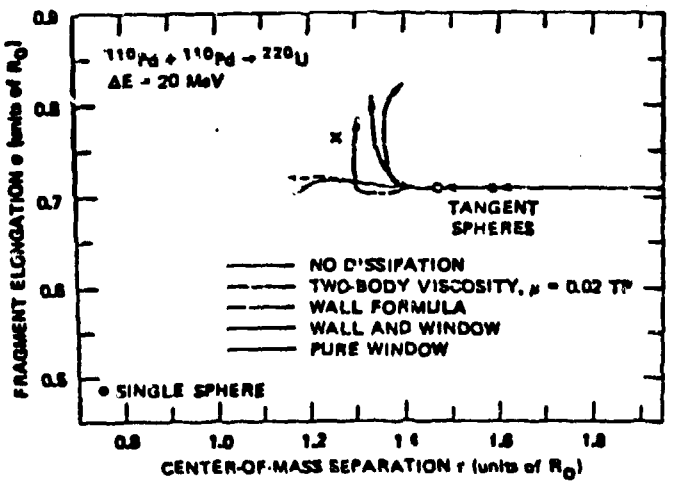

FIGURE 4 Effect of dissipation on dynamical trajectories in the r-σ plane for the reaction $^{110}Pd + ^{110}Pd \rightarrow ^{220}U$ at ΔE = 20 MeV and L = 0, in the full three-quadratic-surface parametrization.[12]

than neck formation σ. On the other hand, all of the one-body dissipation models generate trajectories in which σ changes much more rapidly than r. The result is that for ΔE = 20 MeV fusion occurs only for no dissipation and two-body viscosity. For the one-body dissipation models the system strongly resists compound nucleus formation. Table I shows a comparison of the energy thresholds for the four main dissipation models.

We next study the effect of constraining the end bodies to be spherical; i.e. both the first and third surfaces in the three-quadratic surface parametrization[12] are forced to be spheres throughout the full dynamical evolution. It is very important to study this approximation since it has been widely used in many other macroscopic models.[2-4] In Fig. 5 we show the trajectories for the four main types of dissipation at ΔE = 20 MeV. The most dramatic change is for two-body viscosity, whose trajectory leads to more compressed shapes than the corresponding trajectory when the spherical constraint is not imposed. The third column of Table I lists the threshold ΔE when the ends are constrained to be

TABLE I Calculated additional energy ΔE relative to the maximum in the one-dimensional interaction barrier required to form a compound nucleus in a head-on collision for $^{110}Pd + {}^{110}Pd \rightarrow {}^{220}U$.

Type of dissipation	ΔE (MeV)	
	Full three-quadratic-surface parametrization	Spherical ends
No dissipation	1.5 ± 0.2	4.5 ± 0.1
Two-body viscosity	5 ± 0.5	0.5 ± 0.5
Wall formula	90 ± 2	60 ± 2
Wall and window	39 ± 0.5	32 ± 0.5

DYNAMICAL FUSION THRESHOLDS

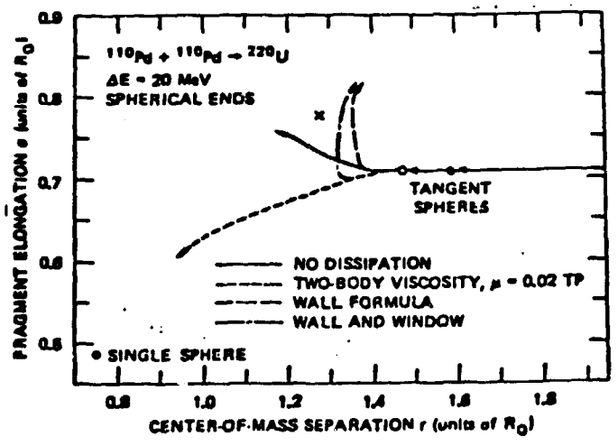

FIGURE 5 Effect of dissipation on dynamical trajectories in the r-σ plane for the reaction $^{110}Pd + ^{110}Pd \rightarrow ^{220}U$ at ΔE = 20 MeV and L = 0, when the end bodies are constrained to be spherical.

spherical. You see that there can be substantial discrepancies arising from the approximation of using spherical end bodies. In particular, for the wall formula the additional threshold energy ΔE is about 30 MeV larger when the spherical constraint is not imposed.

We now show the effect of changing the charge or angular momentum of the system. In Fig. 6 we show dynamical trajectories and saddle points for different values of Z^2/A of the total system. As the charge on the system increases, the saddle point moves to a more compact configuration while the trajectory is deflected in the opposite direction. Thus it becomes more difficult to satisfy the fusion criterion as the charge on the system increases. Note that for Z^2/A = 38.7 the trajectory just passes through the saddle point for a very small ΔE value, so that, for two-body viscosity, Z^2/A = 38.7 is essentially the threshold value.[2-4] The effect of angular momentum is qualitatively similar to that of charge

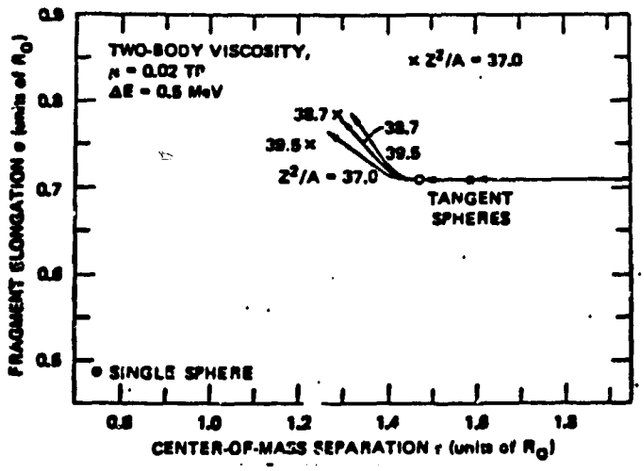

FIGURE 6 Effect of the nuclear system on saddle-point configurations and dynamical trajectories in the r-σ plane for ΔE = 0.5 MeV and L = 0, calculated for two-body viscosity. Each saddle point and trajectory is labeled by the value of Z^2/A for the combined system, with the symmetric target and projectile chosen to lie along Green's approximation to the valley of β-stability.[20]

regarding the behavior of saddle points and dynamical trajectories,[1-4] as we show in Fig. 7. We see that it is more difficult to achieve fusion as the angular momentum increases since the saddle point moves downward and to the left while the dynamical path is shifted to the right.

We now consider the fissilities, or equivalently the Z^2/A values, which are applicable to different regions of our configuration space. For the entrance channel, in the region near contact, the appropriate Z^2/A value is given by the expression,[2-4]

$$(Z^2/A)_{eff} = \frac{4Z_1Z_2}{A_1^{1/3}A_2^{1/3}(A_1^{1/3} + A_2^{1/3})} \qquad (7)$$

However, as the system attains a more coalesced shape, Eq.

DYNAMICAL FUSION THRESHOLDS

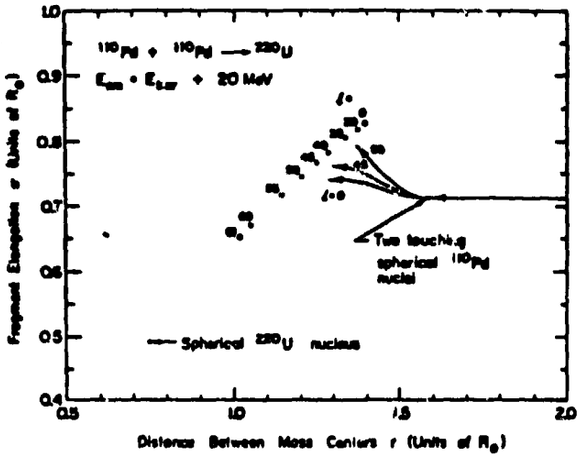

FIGURE 7 Effect of angular momentum on saddle-point configurations and dynamical trajectories in the r-σ plane for ΔE = 20 MeV and zero dissipation.[1] The nuclear macroscopic energy is the single-Yukawa model.[14] Various angular momenta label the trajectories and saddle points, with the latter indicated by circles. The dashed trajectory refers to the critical angular momentum ℓ = 45, above which there is no fusion.

(7) is no longer adequate. Instead, in the region near the saddle point, the appropriate Z^2/A value is that of the total system. For the entire dynamical fusion process, we have found empirically that it is convenient to use the geometrical mean

$$(Z^2/A)_{mean} = [(Z^2/A)_{eff}(Z^2/A)]^{1/2} \tag{8}$$

which gives equal weighting to the entrance-channel and coalesced-shape values. We note too that for mass-symmetric reactions we have the identity

$$(Z^2/A)_{eff} = (Z^2/A) = (Z^2/A)_{mean}. \tag{9}$$

In Fig. 8 we compare our calculated results[5] with the

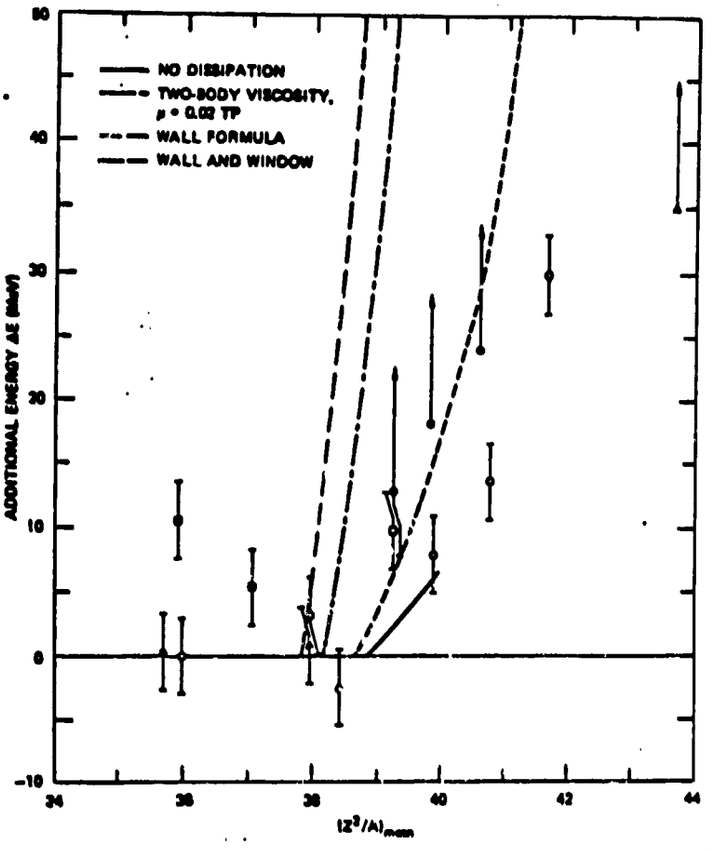

FIGURE 8 Comparison of additional energy ΔE required for compound-nucleus formation calculated for symmetric systems with experimental values for asymmetric systems characterized by $(Z^2/A)_{mean}$, defined by Eq. (8). Values extracted from evaporation-residue measurements are represented by solid symbols, whereas values extracted from measurements of nearly symmetric fission-like fragments are represented by open symbols. (See Ref. 5 for the experimental references.)

experimental data. We plot the calculated threshold ΔE vs $(Z^2/A)_{mean}$ for each of the four main types of viscosity considered. The one-body dissipation results are an order of magnitude greater than those for zero dissipation or two-body viscosity. Since the experiments are for

mass-asymmetric reactions, we have tried to approximately scale the data to compare with our theoretical results for mass-symmetric reactions. This is accomplished by using the geometric mean Z^2/A, defined in Eq. (8). For both the solid and open symbols, the experimental values of the additional energy ΔE are determined by subtracting from the experimental barrier heights extrapolated values that correctly reproduce the smooth trends for somewhat lighter nuclei. The experimental values appear to be in better agreement with the results for two-body viscosity than with the results for either type of one-body dissipation. However, mainly because the error bars on the three highest solid symbols extend to + ∞, any conclusions regarding the nuclear dissipative mechanism must be regarded as very tentative.

4. TDHF RESULTS

We shall now discuss some TDHF results which can be interpreted as the microscopic analogue of the macroscopic extra push. However, we emphasize that the origin of dissipation is different in microscopic theories than in any of the macroscopic viscosity models.[11] In particular, the TDHF dissipation arises only from one-body collisions with the mean-field potential.

Typical fusion results for heavy systems are illustrated in Fig. 9. These calculations[8,9] were performed for head-on collisions of $^{86}Kr + ^{139}La$. The interaction time is plotted vs the laboratory bombarding energy. The interaction time is defined as the time interval during which the density in the overlap region between the coalesced ions exceeds one-half the saturation density of nuclear matter. The most striking feature noticed is that there are two

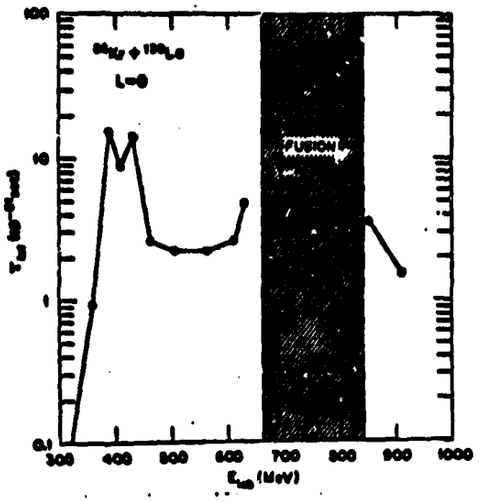

FIGURE 9 The interaction time versus the laboratory bombarding energy for head-on collisions of ^{86}Kr + ^{139}La. The open circles are the results of the TDHF calculations. The shaded area shows the higher-energy fusion region. The calculations were performed using the Skyrme II interaction.

energy regions where one finds fusion-like behavior. In the low-energy region near the interaction barrier one observes three long-lived configurations. Then for energies from $E_{lab} \approx 660$ to ≈ 840 MeV we find true fusion in the sense that, as far as we can determine from the calculations, the system never comes apart. The fusion threshold at $E_{lab} \approx 660$ MeV is the direct analogue of the macroscopic dynamical fusion threshold discussed in Section 3. Above $E_{lab} \approx 840$ MeV, fusion abruptly disappears for head-on collisions; this is the angular momentum window, which is a dynamical fusion threshold found only in TDHF studies.

We emphasize too that the long-lived configurations observed near the barrier are <u>not</u> true fusion cases since each eventually undergoes scission after $\sim 10^{-20}$ sec. They do

not correspond to fast fission[2] either because the final masses and charges of the reaction products are very close to those of the incident projectile and target. Since there is a fluctuating structure observed in this energy region, one suspects that such a reaction may correspond to some type of long-lived molecular resonance. Also, it is interesting that such fusion-like behavior near the barrier is very reminiscent of the adiabatic slither, or cold fusion, predicted recently by Swiatecki.[3]

The higher-energy fusion region is in very poor agreement with the experimental results,[21] for which fusion is found at laboratory bombarding energies of 505, 610, and 710 MeV. In the TDHF calculations,[7-9] fusion does not occur for any angular momentum at the lower two experimental energies, but it does occur for a range of angular momenta at the highest experimental energy (710 MeV).

However, the TDHF fusion behavior is very sensitive to the choice of the effective two-body interaction. For the studies shown in Fig. 9, the Skyrme II potential was used. In recent TDHF studies[22] of $^{86}Kr + ^{139}La$, it is found that if one uses the Skyrme III interaction, the extra-push threshold in Fig. 9 is decreased to $E_{lab} \lesssim 410$ MeV. This is a change of at least 250 MeV, which is a very large effect! Figure 10 displays the rms radius of the total system as a function of time for these two Skyrme forces.[9] For the Skyrme II potential, the rms radius decreases to a minimum value, after which it increases indefinitely as the system reseparates. On the other hand, the rms radius for Skyrme III decreases to a minimum and then increases to a maximum, after which it is dramatically damped in a highly coalesced state. Clearly, additional studies with Skyrme III and other forces must be pursued in order to quantify the TDHF

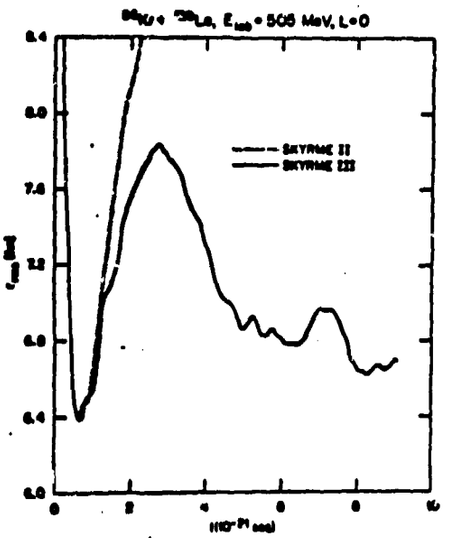

FIGURE 10 The rms radius of the total system as a function of time for head-on collisions of $^{86}Kr + ^{139}La$ at E_{lab} = 505 MeV. The interactions used are the finite-range Skyrme potentials.

fusion behavior of heavy systems. In fact, it has recently been suggested[11] that the modified Skyrme M interaction should be examined since it gives the correct nuclear compressibility and reproduces experimental fission-barrier heights.

Table II shows yet another example of the sensitivity of TDHF fusion behavior to the effective two-body interaction. TDHF calculations have been performed for head-on collisions of $^{160} + ^{160}$, in which the threshold for the relatively high-energy TDHF angular momentum window has been determined for a variety of Skyrme forces.[22] The force labeled BGK was a very simplified Skyrme force used in the Bonche, Grammaticos, and Koonin paper.[23] For the other Skyrme forces, the error bars on the threshold energies indicate the precision with which the fusion window has been

TABLE II TDHF studies of the fusion window for head-on collisions of $^{16}O + ^{16}O$.

Skyrme force	Laboratory threshold energy (in MeV) for the window
BGK	54
II	62.5 ± 2.5
III	57.5 ± 2.5
IV	42.5 ± 2.5
V	52.5 ± 2.5
VI	52.5 ± 2.5

determined. Notice that there are rather large differences in the various threshold energies, ranging from 42.5 MeV for Skyrme IV to 62.5 MeV for Skyrme II. Also, it should be pointed out the experiment of Lazzerini et al.[24] was done at a laboratory energy of 68 MeV, which is only 3-8 MeV above the limits for the Skyrme II threshold. Since the results of these measurements seemed to rule out the existence of the window, it is suggested that it might be desirable to do this experiment again at a somewhat higher energy.

5. SUMMARY

We now summarize the main results. Effects of the extra-push mechanism are predicted by both macroscopic and microscopic theories and include the following. Above a certain critical fissility, fusion cannot occur until the bombarding energy reaches a threshold value which is greater than the entrance-channel interaction barrier height. In order to understand heavy-ion fusion, one must take into account properties of both the entrance channel and the saddle-point regions of configuration space. Also, the macroscopic

results are quite sensitive to some of the details of the model. For example, there can be substantial discrepancies between the thresholds calculated with different shape parametrizations. However, the main uncertainty in the macroscopic work is the nature of the dissipation mechanism since the results for one- and two-body viscosity are clearly very different. Finally, in the microscopic TDHF studies both the extra-push threshold and the angular momentum window seem to be very sensitive to the choice of the effective two-body interaction.

REFERENCES

1. J. R. NIX and A. J. SIERK, Phys. Rev. C 15, 2072 (1977).
2. W. J. SWIATECKI, Phys. Scr. 24, 113 (1981).
3. W. J. SWIATECKI, Nucl. Phys. A376, 275 (1982).
4. S. BJØRNHOLM and W. J. SWIATECKI, Nucl. Phys. A391, 471 (1982).
5. K. T. R. DAVIES, A. J. SIERK, and J. R. NIX, to be published in Phys. Rev. This paper contains additional theoretical and experimental references relevant to dynamical fusion thresholds.
6. P. BONCHE, K. T. R. DAVIES, B. FLANDERS, H. FLOCARD, B. GRAMMATICOS, S. E. KOONIN, S. J. KRIEGER, and M. S. WEISS, Phys. Rev. C 20, 641 (1979).
7. K. T. R. DAVIES, K. R. S. DEVI, and M. R. STRAYER, Phys. Rev. C 20, 1372 (1979).
8. K. T. R. DAVIES, K. R. S. DEVI, and M. R. STRAYER, Phys. Rev. Lett. 44, 23 (1980).
9. K. T. R. DAVIES, K. R. S. DEVI, and M. R. STRAYER, Phys. Rev. C 24, 2576 (1981).
10. H. STÖCKER, R. Y. CUSSON, H. J. LUSTIG, A. GOBBI, J. HAHN, J. A. MARUHN, and W. GREINER, Z. Phys. A306, 235 (1982).
11. J. R. NIX, to be published in Comments on Nuclear and Particle Physics.
12. J. R. NIX, Nucl. Phys. A130, 241 (1969).
13. K. T. R. DAVIES, A. J. SIERK, and J. R. NIX, Phys. Rev. C 13, 2385 (1976).
14. P. MÖLLER and J. R. NIX, Nucl. Phys. A272, 502 (1976).

15. H. J. KRAPPE, J. R. NIX, and A. J. SIERK, Phys. Rev. Lett. 42, 215 (1979).
16. H. J. KRAPPE, J. R. NIX, and A. J. SIERK, Phys. Rev. C 20, 992 (1979).
17. A. J. SIERK and J. R. NIX, Phys. Rev. C 21, 982 (1980).
18. J. BŁOCKI, Y. BONEH, J. R. NIX, J. RANDRUP, M. ROBEL, A. J. SIERK, and W. J. SWIATECKI, Ann. Phys. (N.Y.) 113, 330 (1978).
19. J. RANDRUP and W. J. SWIATECKI, Ann. Phys. (N.Y.) 125, 193 (1980).
20. A. E. S. GREEN, Nuclear Physics (McGraw-Hill, New York, 1955), pp. 185, 250.
21. P. DYER, M. P. WEBB, R. J. PUIGH, R. VANDENBOSCH, T. D. THOMAS, and M. S. ZISMAN, Phys. Rev. C 22, 1509 (1980).
22. K. T. R. DAVIES, J. A. MARUHN, and M. R. STRAYER, to be published.
23. P. BONCHE, B. GRAMMATICOS, and S. E. KOONIN, Phys. Rev. C 17, 1700 (1978).
24. A. LAZZARINI, H. DOUBRE, K. T. LESKO, V. METAG, A. SEAMSTER, R. VANDENBOSCH, and W. MERRYFIELD, Phys. Rev. C 24, 309 (1981).